Received: 27 January 2023 | Revised: 19 April 2023 | Accepted: 4 May 2023

DOI: 10.1002/jbm.a.37557

RESEARCH ARTICLE

Skin substitutes based on gellan gum with mechanical and penetration compatibility to native human skin

Deepika Malhotra[1] | Ehsan Fattahi[1] | Natalie Germann[2] | Tatiana Flisikowska[3] | Angelika Schnieke[3] | Thomas Becker[1]

[1]TUM School of Life Sciences Weihenstephan, Chair of Brewing and Beverage Technology, Fluid Dynamics Group, Technical University of Munich (TUM), Freising, Germany

[2]Faculty 4 – Energy-, Process- and Bioengineering, Chair of Process Systems Engineering, University of Stuttgart, Stuttgart, Germany

[3]TUM School of Life Sciences Weihenstephan, Chair of Livestock Biotechnology, Technical University of Munich (TUM), Freising, Germany

Correspondence
Ehsan Fattahi, TUM School of Life Sciences Weihenstephan, Chair of Brewing and Beverage Technology, Fluid Dynamics Group, Technical University of Munich (TUM), Freising 85354, Germany.
Email: ehsan.fattahi@tum.de

Natalie Germann, Faculty 4 – Energy-, Process- and Bioengineering, Chair of Process Systems Engineering, University of Stuttgart, Stuttgart 70199, Germany.
Email: natalie.germann@svt.uni-stuttgart.de

Funding information
TUM

Abstract

The study reports on a simple system to fabricate skin substitutes consisting of a naturally occurring bacterial polysaccharide gellan gum. Gelation was driven by the addition of a culture medium whose cations induced gellan gum crosslinking at physiological temperature, resulting in hydrogels. Human dermal fibroblasts were incorporated in these hydrogels and their mechanical, morphological, and penetration characteristics were studied. The mechanical properties were determined by means of oscillatory shear rheology, and a short linear viscoelastic regime was noted up to less than 1% of strain amplitude. The storage modulus increased with an increasing polymer concentration. The moduli were in the range noted for native human skin. After 2 weeks of fibroblast cultivation, the storage moduli showed signs of deterioration, so that a culture time of 2 weeks was proposed for further studies. Microscopic and fluorescent staining observations were documented. These depicted a crosslinked network structure in the hydrogels with a homogeneous distribution of cells and an assured cell viability of 2 weeks. H&E staining was also performed, which showed some traces of ECM formation in a few sections. Finally, caffeine penetration experiments were carried out with Franz diffusion cells. The hydrogels with a higher concentration of polymer containing cells showed an improved barrier function against caffeine compared to previously studied multicomponent hydrogels as well as commercially available 3D skin models. Therefore, these hydrogels displayed both mechanical and penetration compatibility with the *ex vivo* native human skin.

KEYWORDS
gellan gum, human dermal fibroblasts, human skin, hydrogel, penetration properties, skin substitutes, viscoelasticity

1 | INTRODUCTION

Polysaccharides are easily available, naturally occurring materials that are both biocompatible and biodegradable. They are mechanically stable and functionally tuneable due to the presence of several functional groups. Their hydrophilicity makes them a contender to form porous and fibrillar hydrogels that can act as scaffolds in the application of wound dressings and tissue engineering.[1] Hydrogels are the most promising biomaterial for cell culture as they possess a 3D structure, their water content facilitates circulation, they display

similar soft tissue mechanics, are very similar to the native extracellular matrix (ECM) and support cell adhesion.[2,3]

Gellan gum is an extracellular bacterial (*Sphingomonas elodea*) polysaccharide with linear, anionic, tetrasaccharide repeating units composed of D-glucose, L-rhamnose and D-glucuronic acid (2:1:1), linked by a β $(1 \rightarrow 4)$ glycosidic bond. It possesses a coaxial double helical (left-handed) structure in its solid state with the two chains running parallel. At high temperatures, it exists as a viscous solution in water (ca. 85°C) with coils in a disordered state. When cooled down, it assumes an ordered, double helical configuration and forms a weak gel. These helical entities must be aggregated to obtain a stronger hydrogel. This can be achieved by adding cations, because gellan gum has a net negative charge due to the presence of carboxylic groups.[4] There are several advantages of employing gellan gum as a tissue engineering scaffold, some of which are: its 3D structure allows greater proximity to the native arrangement; its ability to form hydrogels ensures enough nutrient and waste circulation; it can crosslink with a standard cell culture medium containing only a low concentration of cations, which is conductive for cell cultivation and poses no threat to the incorporated cells. These features make gellan gum perfect for scaffolding.[5,6] Gellan gum-based hydrogels or composite scaffolds have been applied for intervertebral disc and skeletal muscle tissue engineering, the dispersion of neural stem/progenitor cells (NSPCs), peripheral nerve regeneration, the promotion of fibroblast differentiation, skin wound healing, bone and cartilage tissue engineering and potential osteogenesis.[7–14] Hence, gellan gum is a promising candidate for applications in the field of tissue engineering of human tissues, such as skin.

In tissue engineering and regenerative medicine, the evaluation of the mechanical properties of scaffolds and matrices is an important criterion when studying these materials because their rigidity influences cell differentiation and matrix stiffness plays a role in mediating cell behavior.[15,16] When it comes to skin, the largest and outermost tissue of humans, its substitutes need to be sufficiently elastic to withstand the physiological loads and biological forces.[17] Native human tissues, such as skin, are viscoelastic by nature and can be mechanically studied by oscillatory rheology.[18–23] It is therefore important to assess the viscoelastic behavior of hydrogels that function as skin scaffolds so as to resolve the failure issues of currently available options.[24–26]

In the cosmetics and pharmaceuticals industry, an assessment of the transdermal delivery of topical application products such as drugs, toxins and cosmetics, is important to test their permeation via the skin. For this purpose, *ex vivo* animal or human skin is employed, and the penetration characteristics of the products are determined through the skin. The number of human skin samples donated for research purposes is limited, and animal testing has to be alleviated. Thus, it becomes necessary to develop and know the barrier function of skin substitutes and then compare this to their native counterpart to see if they show a similar pattern.[27,28] As yet, there have been no systems that match the native skin very well. Consequently, there are constant efforts to find a suitable alternative.[29,30] Human skin-like tissue engineering began in the 1990s, when epidermal and dermal layers were developed *in vitro* in hyaluronic acid-derived biomaterials.[31] This idea has now been further developed into the commercially available 3D reconstructed full-thickness skin models (Phenion® FT model), which show a higher transdermal permeation activity than both human and animal skins.[32] As for hydrogel-based scaffolds, our previous work has shown that the penetration rate of a caffeine solution through these multicomponent hydrogels ranges between 12.89% and 42.33% after 6 h, depending on the different concentrations of κ-carrageenan present in them. On the other hand, only 4.25% of caffeine penetrated native human skin in the same time interval. We also compared these results with the 3D reconstructed skin models and observed a caffeine penetration rate of 22.66%.[26] Therefore, these substitutes possess a lower barrier function than their human counterpart. Consequently, our current study becomes quite useful, not only to replace human and animal testing, but also to achieve a better, more cost-effective and easy-to-fabricate alternative that displays a penetration behavior comparable to that of native skin.

This work investigates the applicability of gellan gum-based hydrogels as skin scaffolds, with both a mechanical and penetration compatibility to the native human benchmark. We previously performed this study with the hydrogel scaffold. In this study, we introduced the culture of human dermal fibroblasts in gellan gum hydrogel scaffolds to get closer to the real *in vivo* environment. The article is divided up into the following sections: the following section, that is, Section 2, presents the protocols for hydrogel preparation (with and without the incorporation of human dermal cells), oscillatory rheology, cell viability assessment, microstructure, and diffusion experiments. In Section 3, we report on and discuss the results of all the conducted studies and compare them to the native counterpart, commercially available 3D reconstructed skin models and previously studied hydrogels. Section 4 provides a summary of the main conclusions.

2 | MATERIALS AND METHODS

2.1 | Hydrogel preparation

Gellan water solutions (GWS) of different concentrations (w/w) were prepared by dispersing powdered low acyl gellan gum (Gelzan™ CM, Sigma-Aldrich) in deionized water. The method we adopted was that of Moxon et al.,[5] with additional procedural improvements. Gellan gum was dissolved in water by gentle stirring for 20 min at 85°C in a closed-cap bottle to avoid water loss by evaporation. Following complete dissolution, the temperature of the heating plate was reduced to 37°C and maintained for 30 min before the next steps. Parallel to this, unsupplemented medium (containing cations for crosslinking), that is, Dulbecco's Modified Eagle Medium (DMEM) (Sigma-Aldrich) was also maintained at 37°C. The desired volumes of both GWS and DMEM were pipetted into a small preheated beaker (also around 37°C) and mixed gently by pipetting the components in and out for a few times. The beaker was tapped lightly to eliminate any air bubbles, if any. Hydrogel began to form rapidly and was completed after the beaker was left at room temperature for 30 min. The beaker was then tilted slightly and the gel was gently pushed out into a petri dish with the help of a spatula. Hydrogel with a diameter of 15 mm was obtained using a stainless-steel puncher (also used previously in Reference 26).

	GWS (wt %)	GWS:DMEM (v/v)	Sample Name	Reference
(A)	1.5 wt %	1:2	Gellan 1:2, Gellan 1:2 w NHDF	Current work
		1:1	Gellan 1:1, Gellan 1:1 w NHDF	

	Skin source/type	Age [years] or age group	Body location	Sample code	References
(B)	Male human skin	23	Abdomen	23MWS	22,33
	3D skin models	Juvenile	Foreskin	3DFTJV	

	Composite hydrogels with κ-Carrageenan (wt %	Sample name	Reference
(C)	0.3 wt %	κ-Carr 0.3 wt %	26
	0.5 wt %	κ-Carr 0.5 wt %	
	0.8 wt %	κ-Carr 0.8 wt %	

TABLE 1 Composition of the hydrogels studied in this work (A), along with the details of the native human skin and 3D skin models (B) and previously studied hydrogels (C), used for comparison.

Note: (A) *Sample names*: The ratio in the front represents GWS:DMEM volume ratio, where GWS refers to Gellan Water Solution, and DMEM is the abbreviation for Dulbecco's Modified Eagle's Medium.
(B) *Sample codes*: **Male Human Skin:** The initial two digits "23" denote the skin donor's age in years, "M" represents the male gender and "WS" denotes the whole skin (epidermis and dermis). **3D Skin Models:** "3D" denotes the three-dimensional reconstruction of the model, "FT" represents full-thickness, comprising epidermis and dermis and "JV" denotes the juvenile age-group of the donor from whose skin, cells were isolated to construct this model.
(C) *Sample names*: κ-Carr refers to κ-carrageenan with its varying concentrations in wt % (w/w%) in the gel mixtures for fabricating hydrogels, while keeping the concentration of the rest of the components constant.

This size fit into the rheological measurement system. The most suitable concentrations of GWS and ratios of GWS-DMEM mixtures are shown in Table 1.

Figure S1A–D in Section A of the Supplementary Information (SI) shows the experimental procedure for preparing the hydrogels in detail.

2.2 | Hydrogels with incorporated normal human dermal fibroblasts (NHDF)

To optimize the procedure for the preparation of hydrogels with cells, initial trials were carried out with porcine kidney cell line (PK-15). Following optimization, normal human dermal fibroblasts (NHDF – Adult, C-12302 from PromoCell, Merck) were initially cultured in a T75 (passage 2) flask in Fibroblast Growth Medium 2 (FGM2, C-23020 from PromoCell, Merck). This already contained the required supplements after mixing with SupplementMix provided with the product, as instructed by the supplier. The cultivated cells were detached with accutase (A6964 from Sigma-Aldrich) after at least 70% confluency, following the standard protocol. The detached cells were expanded and cultured in T150 (passage 3) flasks at a cell density of 5×10^3 cells cm^{-2} and cultivated until at least 70% confluency, with a change of medium every two to 3 days. NHDF were then cryopreserved in supplemented FGM2 medium with 10% DMSO. Cryopreserved cells were thawed, cultivated, detached and used for hydrogels cultivation when they were in passage 4 or 5. The cell solution for hydrogels was prepared in supplemented FGM2, mixed with the required amount of DMEM (all maintained at 37°C), and finally pipetted into the already prepared hydrogel solution (GWS), as explained in Section 2.1, at 37°C. The final concentration of NHDF was maintained at 1.25×10^5 cells mL^{-1} in the hydrogel, at a ratio of 1:10 v/v of NHDF:GWS, as followed by Moxon and Smith.[5] The hydrogels with and without NHDF cells were cultured in 6-well plates, and FGM2 with the required supplements was used for cultivation with the addition of 1% v/v Penicillin-Streptomycin to prevent contamination. The medium was changed every 2 days. After two and 3 weeks of cultivation, hydrogels were ready for rheological, microstructural and penetration studies. The 6-well plates with cultured hydrogels are shown in Figure S1E in Section A of the SI file.

2.3 | Studying rheological behavior

A stress-controlled conventional rheometer (Physica MCR 502, Anton Paar, Graz) with stainless-steel, smooth parallel plates was used for the oscillatory shear measurements. Both fixed (lower) and oscillating (upper) plates had a diameter of 15 mm. The average gap width was 1.92 ± 0.60 mm depending on the sample height. All measurements were carried out at 37°C. Further steps to maintain the humidity, adjust normal force and thermal equilibrium were performed as described in our previous articles.[22,26] We studied the hydrogels under the small amplitude oscillatory shear, that is, SAOS, as described in our previous articles. The strain amplitude (γ) sweep ($0.01\% < \gamma < 2.0\%$) at a constant angular frequency (ω) of 0.5 rad s^{-1} was followed by an angular frequency sweep ($0.1 < \omega < 5$ rad s^{-1}) at a constant strain amplitude (chosen well within the linear viscoelastic [LVE] region) to study the intracycle shear response. All tests were performed in triplicate ($n = 3$). Figure S2 in Section A of SI shows the hydrogel placed in the rheometer geometry.

2.4 | Live cell staining and microscopic imaging

To ensure cell viability, calcein AM, a dye permeable to living cells, was used as an indicator of cell viability. 10 µL aliquots of calcein AM (Cayman Chemical, USA) were prepared in DMSO (under sterile conditions) at a concentration of 1 mM and stored at −20°C. After 2 and 3 weeks of cell culture in hydrogels with NHDF, the culture medium was aspirated from the wells and the hydrogels were washed with PBS. One aliquot was taken for each well, thawed, mixed in 1 mL of culture medium and pipetted into the well to achieve a final calcein AM concentration of 10 µM. After 30 min incubation at 37°C, the calcein AM was replaced by PBS and viewed under a fluorescence microscope (Leica Microsystems, Germany). The absorption and emission maxima of 494 nm (blue) and 517 nm (green), respectively, were used to produce the images in LAS X software. After 3 weeks of cultivation, a deterioration was observed in the mechanical properties and cell viability. Therefore, 2 weeks of culture were chosen for the further characterization (microscopic observations, hematoxylin and eosin staining, penetration studies, and caffeine quantification).

After 2 weeks *in vitro* cultivation of fibroblasts, hydrogel samples were viewed under an inverted light microscope (Leica Microsystems, Germany) and images were taken at different overall magnifications of 50×, 100×, and 200× using the LAS X software.

2.5 | Hematoxylin and eosin staining

The culture medium was aspirated after 2 weeks of cultivating the hydrogels. These were then placed in chambers and soaked in a sufficient amount of freshly prepared 4% paraformaldehyde (PFA) for 1 day. The next day, PFA was replaced by 70% ethanol, until the dehydration and paraffin embedding step was carried out. Thereafter, the embedded samples were cooled to −20°C for at least a couple of hours before slicing them in a microtome. 2–10 µm slices were collected on glass slides and dried as per the standard protocol. This was followed by hematoxylin and eosin (H&E) staining of the samples, this being the staining method used for routine diagnosis and tissue structure in histology.

2.6 | Penetration study

Vertical, Franz-type static diffusion cells (FDC, PermeGear Europe, SES GmbH Analysesysteme, Germany) were used to analyze the penetration properties of caffeine through the barrier created by the fabricated hydrogels (after 2 weeks of cultivation). More details of the FDC setup and protocol can be found in Section B and Figure S3 of SI. 300 µL of the receptor fluid were sampled at 0, 2, 4, and 6 h and samples were stored at −20°C immediately until HPLC analysis. All tests were performed in triplicate ($n = 3$) with all three cells operating simultaneously. Methanol and deionized water were used at ambient conditions for cleaning in two consecutive cycles, both before and after measurements. The procedure was performed according to the OECD 428 guidelines.

2.7 | Caffeine quantification

A fully automatic, High Performance Liquid Chromatography (HPLC) system from Dionex (U3000) was used. This was equipped with a high-pressure quaternary pump, a Dionex DAD-detector as well as a Phenomenex precolumn combined with a reverse-phase column type Phenomenex Gemini 5 µm, C18, 150 mm × 4.6 mm. It was used for caffeine detection at a wavelength of 273 nm. The mobile phase consisted of an aqueous solution of potassium dihydrogen phosphate (5.44 g L^{-1}) adjusted with phosphoric acid to a pH of 2.5 and degassed in ultrasound for 5 min. The flow rate was set to 1 mL min^{-1} with an average retention time of 4.65 min. The detection limit was 0.05 µg mL^{-1}. For the analysis, 20 µL of the solution were injected and a total run time of 16 min was used for each sample. Before the actual experiment, we successfully established a calibration curve with a linear range of 0.05–50 µg mL^{-1} caffeine. We analyzed the penetration flux of caffeine across the samples as a function of time after 6 h.

2.8 | Statistical analysis

Results are reported as a mean ± standard deviation ($M \pm SD$) indicating an average of three samples ($n = 3$)., A statistical analysis in OriginLab software was used for a group comparison, employing the one-way ANOVA (analysis of variance) method. The significance level between groups was set as $^{*}p < .05$, $^{**}p < .01$, $^{***}p < .001$, $^{****}p < .0001$, $^{*****}p < .00001$. p-values were considered significant if they were below .05.

3 | RESULTS AND DISCUSSION

3.1 | Viscoelastic properties

The response of different specimens to inter- and intracycle small amplitude oscillatory shear (SAOS) stresses just after cultivation is illustrated in Figure 1A,B, respectively. The SAOS signifies that the rheological behavior remains within the LVE regime. Here we compare the rheological behavior of NHDF-gellan hydrogels from this study with native human skin, commercially available 3D skin models and our previously reported hydrogels.[22,26] The dependence of storage G' (indicative of elastic behavior) and loss G'' (indicative of viscous behavior) moduli on strain amplitude γ is shown in Figure 1A (intercycle strain deformation behavior). The amplitude value up to which the signal was measured, that is, the upper limit of γ, depended on each sample's linear regime range (shorter or longer). Therefore, it is not the same for all samples. Figure 1B shows the progression of the dynamic moduli as a function of angular frequency ω, at a fixed γ in LVE regime (intracycle behavior). The sweeps assumed a similar shape for both tests, both with and without the incorporation of NHDF, with differences in magnitude. Consequently, only the results from NHDF-gellan hydrogels are shown in these figures for better clarity. In all the samples, it could be observed, that the G' remains at an order

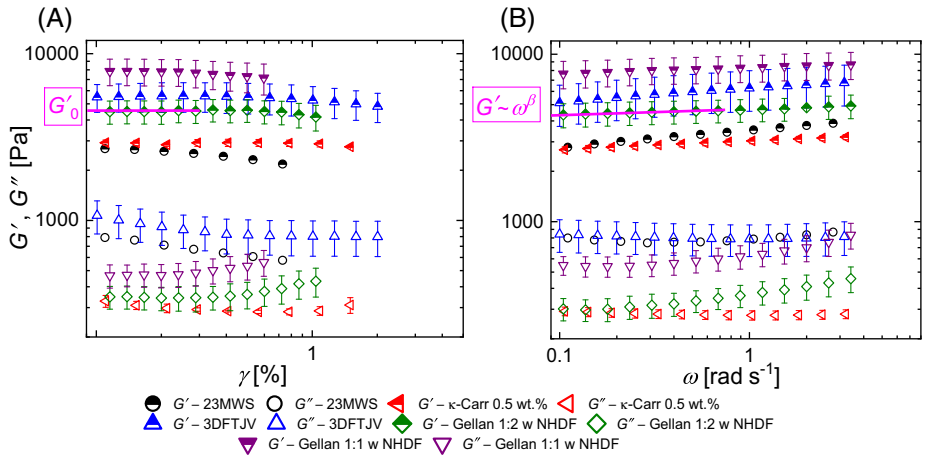

FIGURE 1 Dependency of storage (G′) and loss (G″) moduli on strain amplitude γ [%] at a fixed angular frequency ω of 0.5 rad s^{-1} (A), and on angular frequency ω [rad s^{-1}] at a fixed strain amplitude γ [%] in a linear viscoelastic (LVE) regime, taken from subfigure A (B), for gellan gum hydrogels with incorporated normal human dermal fibroblasts (NHDF) Gellan 1:2/1:1 w NHDF, previously studied hydrogels κ-Carr 0.5 wt %, native human skin 23MWS, and *in vitro* 3D reconstructed skin models 3DFTJV. G'_0 in subfigure A denotes the intrinsic storage modulus derived from the dependence of G' on strain at the limit of zero strain amplitude. β in subfigure B represents the dimensionless power-law exponent derived from the angular frequency dependence of G'. The error bars represent the standard deviation for three measurements ($n = 3$).

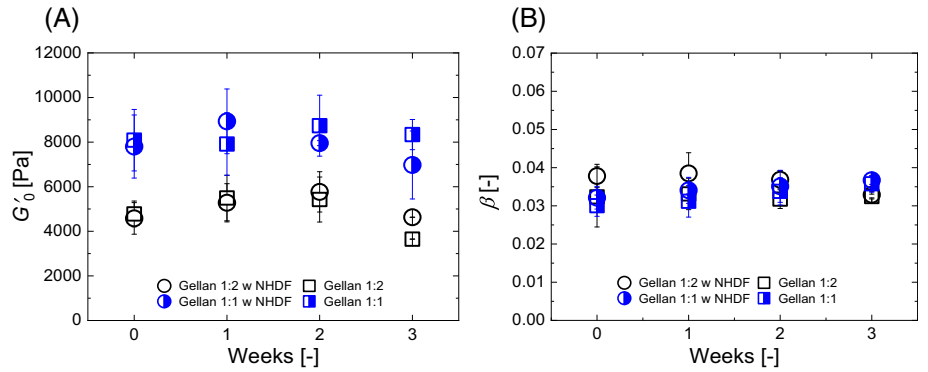

FIGURE 2 (A) G'_0 (intrinsic storage modulus) and (B) β (power-law coefficient of storage modulus) as a function of time for gellan gum hydrogels culture in weeks. G'_0 is estimated by the linear least squares fitting of G' at very low strain amplitudes and represents the y-intercept while extrapolating the data with slope = 0 (see Figure 1A), whereas β is estimated by least squares power-law fitting of G' versus angular frequency, which represents the slope of the same in the log–log plot (see Figure 1B). The error bars represent the standard deviation for three measurements ($n = 3$).

of magnitude higher than the G'' (phase angle <45°) in both Figure 1A,B, and is weakly dependent on the angular frequency. This indicates that the samples show a gel-like rheological behavior. Frequency sweeps describe the time-dependent behavior and correspondingly the inner structure of a material. As shown in Figure 1B, the storage moduli are frequency dependent, whereas the viscous moduli show a more stable response. Also, no crossover is observed in the frequency sweeps for any samples in the tested range. The increase in the moduli, gradual or sharp, with an increasing angular frequency indicates changing intracycle viscoelastic characteristics depending on time. Details of the viscoelastic behavior of multilayered native human skin samples, taking into account dermal and epidermal contributions, and the hydrogels previously studied can be found in our publications from 2019 and 2021.[22,26] It should be noted that the results with gellan samples obtained in our work follow a trend similar to that observed by Moxon and Smith,[5] although the moduli magnitudes differ. This is due to differences in gellan gum, GWS concentration, the final amount of DMEM present and slight differences in the DMEM composition itself.

We use the predominant storage modulus to compare the magnitude of different specimens under intercycle shear. In the LVE regime, the storage modulus is independent of the applied strain amplitude. We refer to this modulus as G'_0, which reveals the inherent elastic strength of a material at a very low strain. This is highlighted in dark pink in Figure 1A. The two main observations can be summarized as follows: (1) all three skin substitutes containing cells being studied here show a storage modulus that is 1.5–3 times higher than the male abdominal benchmark analyzed by us earlier; (2) when we compare both gellan gum hydrogels, the 1:2 sample shows a lower G'_0 of 4.58 kPa, only 0.59 times the G'_0 of the 1:1 sample. Ramaswamy, Jabbarzadeh and

co-workers also reported a higher storage modulus for gellan gum-based hydrogels with a higher polymer concentration.[34] The slope of the storage modulus in frequency sweeps in a log–log plot is considered to determine the comparison of different specimens under intracycle shear. This is referred to as β, the dimensionless power-law exponent. This parameter indicates the dependence of storage modulus on angular frequency. A weaker dependence or lower magnitude of β confirms the presence of a strong gel and elastic rigidity.[19,24] β is related to G' as: $G' \sim \omega^{\beta}$, and is shown in dark pink in Figure 1B.

The parameters G'_0 and β were calculated for gellan gum hydrogels at different cultivation periods and plotted in Figure 2A,B. Figure 2A,B show the G'_0 and β progression respectively, of all the gellan gum samples (1:2 and 1:1), both with and without NHDF, as a function of the culture period. Clearly, in Figure 2A, the samples with a higher gellan concentration, that is, 1:1 samples, show 1.4 to 2.4 times higher magnitudes of G'_0 than the corresponding 1:2 specimens at the same time point. There is no clear trend of an increment or decrement until 2 weeks of culture. The 1:2 samples show almost no difference between the magnitudes of hydrogels with and without dermal fibroblasts. Although the 1:1 sample showed some variations between these two, however, these were not consistent, that is, after 1 week, the samples with cells were higher, and after 2 weeks, the hydrogels without NHDF showed greater values of G'_0. As can be seen in Figure 2B, the magnitude of the power-law exponent β does not change much with samples or over time, and stays between 0.032 and 0.039 ± 0.005. β for samples with cultivated NHDF only remains slightly higher than the samples without cells for the entire culture duration. The power-law exponent β shows neither noticeable differences nor a specific trend over culture time of 2 weeks. This means that, in terms of the intracycle behavior at constant strain amplitude, the change in the moduli over angular frequency is almost unaffected by polymer concentration and culture time. This is because the main components did not change in the system, and the frequency sweep is a material fingerprint. A similar observation was noted in our work related to carrageenan-based hydrogels when polymer concentration was changed.[26]

It can be noticed in Figure 2A that the storage modulus of all the samples decreases after 2 weeks of cell culture to a lower value after 3 weeks. This observation could possibly be the result of cell migration, matrix rearrangement or biodegradation of the scaffold.[35] Any of these occurrences can lead to reduction of elasticity as reported by Anseth and co-workers, who used multiple particle tracking microrheology for this purpose.[36] Even in the absence of cells, ion exchange between cations present in the culture medium that crosslink the polysaccharide hydrogel, may result in a reduction in mechanical properties.[37] This phenomenon only becomes visible after 2 weeks when the medium had been exchanged several times. This can be due to the fact that unlike other polysaccharides, gellan gum needs a low concentration of cations to crosslink and form hydrogels. Moreover, both monovalent and divalent cations can perform this function. This means that the impact is only seen after a while under cell culture conditions.[38] This decrement is more pronounced in the samples where a higher proportion of culture medium is present, that is, GWS:DMEM of 1:2, which endorses the

TABLE 2 Comparison of storage moduli and power-law exponents for human skin samples and their substitutes as reported by different literature sources.

Specimen	Age/age group [y]	Gender	Body location	Skin layer	Rheometer geometry	Configuration	Strain amplitude γ [%]	Angular frequency ω [rad s^{-1}]	Temperature [°C]	Storage modulus range [kPa]	Power-law exponent [−]	References
Native human skin	23	Male	Abdomen	WS	Top 8 mm, bottom 15 mm	Parallel plate	0.1–1	0.5 | 0.1–3	37	2.83	0.09	22
	–	–	Foreskin	WS	8 mm	Parallel plate	0.5	0.628–6.283	37	–	0.05	19
	34–54	F	Abdomen	WS	50 mm × 8 mm × 5 mm	Eccentric, at the edge	1	6.28	37	2.5–4.8	–	20
	18–40	F	Mammary	WS	Top 8 mm, bottom 50 mm	Parallel plate	0.01–0.1	6.28	25	4.3–5.8	–	21
	34–54	F	Abdomen	Epidermis	50 mm × 8 mm × 5 mm	Eccentric, at the edge	1	6.28	37	4.6–8.0	–	20
	35–55	F	Abdomen	Epidermis	33 mm, sand blasted	Eccentric, at the edge	1	10	37	4.0–10.0	–	18
3D skin models	Juvenile and aged 3D models	Male	Foreskin cells	FT	Top 8 mm, bottom 15 mm	Parallel plate	0.1–1	0.5 | 0.1–4	37	4.5–7.1	0.061–0.083	22
Hydrogel-based scaffolds	Carrageenan-based hydrogels	–	–	–	40 mm	Parallel plate	1	6.31 | 0.063–631	37	1.8–3.0	0.03–0-07	24
		–	–	–	15 mm	Parallel plate	0.1–2	0.5 | 0.1–3	37	1.9–5.3	0.044–0.051	26

aforementioned reasoning. On the other hand, these influences are not particularly noticeable in Figure 2B, where intracycle stress plays a role. The power-law exponent β remains almost the same for all the samples over a period of 3 weeks. This indicates that such a rearrangement or degradation of the scaffold does not have an impact on the intracycle response of the hydrogels to increasing angular frequency, where the strain amplitude remains constant in the LVE regime.

We now summarize the inter- and intracycle results of human skin and hydrogels from the literature available on similar studies in Table 2. This literature review confirms that the magnitude range of the parameters G'_0 and β obtained in our fabricated skin substitutes falls within or close to the range of the human native skin.

3.2 | Cell viability and hydrogel microstructural insights

Calcein AM assay was used for a rapid evaluation of cell viability in cell culture. A green fluorescence is induced by the hydrolysis of calcein AM during the esterase activity of living cells. In our work, samples were stained with calcein AM after two as well as 3 weeks of cultivation under physiological conditions. Figure 3 shows Calcein AM-stained hydrogel samples after 2 weeks of culture. Subfigures 3A and 3B correspond to the hydrogels with lower (sample 1:2) and higher (sample 1:1) gellan gum concentrations, both containing NHDF, respectively. The specimens without dermal fibroblasts were completely black without any detected fluorescence, and served as controls. The samples with cells appeared green under blue fluorescent light, as shown in Figure 3, ensuring cell viability over time. The cell density in 1:1 samples was observed to be less than that in 1:2 samples. The higher polymer concentration in the hydrogels 1:1, and hence denser network of the gellan gum present here, allows less space for the cells to enter and grow. Therefore, we had a higher cell density in the samples with a 1:2 ratio of gellan gum to DMEM, which had a less dense polymer structure.

The 1:2 specimens after 3 weeks of cultivation showed a lower cell density and higher cell size, as depicted in Figure 4. This could indicate cellular senescence in the primary human dermal fibroblasts from an adult donor. Cell senescence is the irreversible arrest of the cell cycle and is indicative of cell aging. Senescent cells show an enlarged morphology and cease to proliferate. It is important to note that senescent cells secrete a variety of factors that can impact the surrounding microenvironment, including pro-inflammatory cytokines, growth factors, as well as ECM-degrading enzymes.[39] In our study, we observed a deterioration of the hydrogels after 2 weeks of culture, which may be related to the potential effects of cellular senescence on the stability of the original storage moduli values after 2 weeks of culture (see Section 3.1). Therefore, our further characterization was limited to a culture period of 2 weeks for hydrogels incorporated with cells (as indicated in Section 2.4).

The microstructure of native human tissues and their substitutes is an important criterion to a better study of their physiology. The upper (subfigures A, B) and lower (subfigures C, D) panels of Figure 5 show gellan hydrogel samples with and without NHDF respectively, under light microscope, after 2 weeks of culture. A network of mesh-like structures can be observed here. Homogeneity of cross-linked gellan fibers can also be seen in the structure throughout. The left (subfigures A, C) and right (subfigures B, D) panels represent 50× and 200× magnification, respectively. Cells in subfigures C and D appear as round bodies, visible in the forefront or in the background depending on the point in focus, owing to the 3D structure.

Histologically-stained cross-sections viewed under a light microscope have routinely been used to study dermal tissue under normal as well pathological conditions. Hematoxylin and eosin staining,

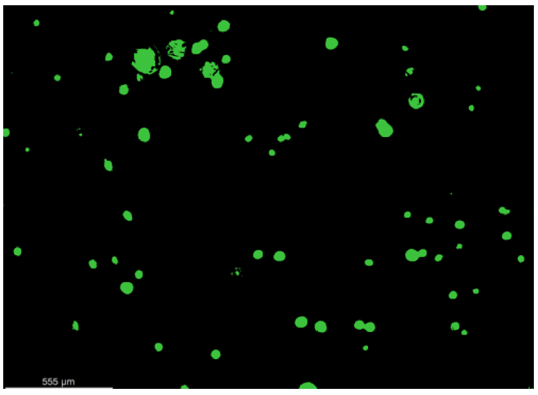

FIGURE 4 Fluorescence microscopic images of Gellan 1:2 hydrogels with NHDF. The hydrogels were kept in a culture for 3 weeks and then stained with calcein AM viability fluorescent dye. The images were magnified 50×, with a scale bar of 555 µm.

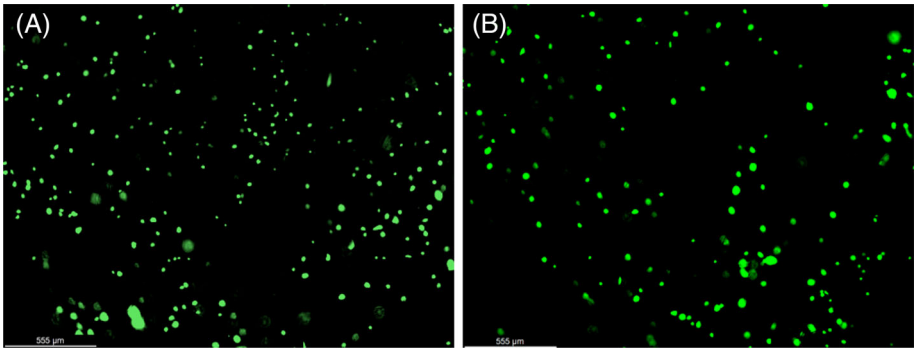

FIGURE 3 Fluorescence microscopic images of Gellan 1:2 hydrogels with NHDF (A), and Gellan 1:1 hydrogels with NHDF (B). The hydrogels were kept in a culture for 2 weeks and then stained with calcein AM viability fluorescent dye. The cell density in 1:1 samples (subfigure B) was observed to be less than that in 1:2 samples (subfigure A). The images were magnified 50×, with a scale bar of 555 µm.

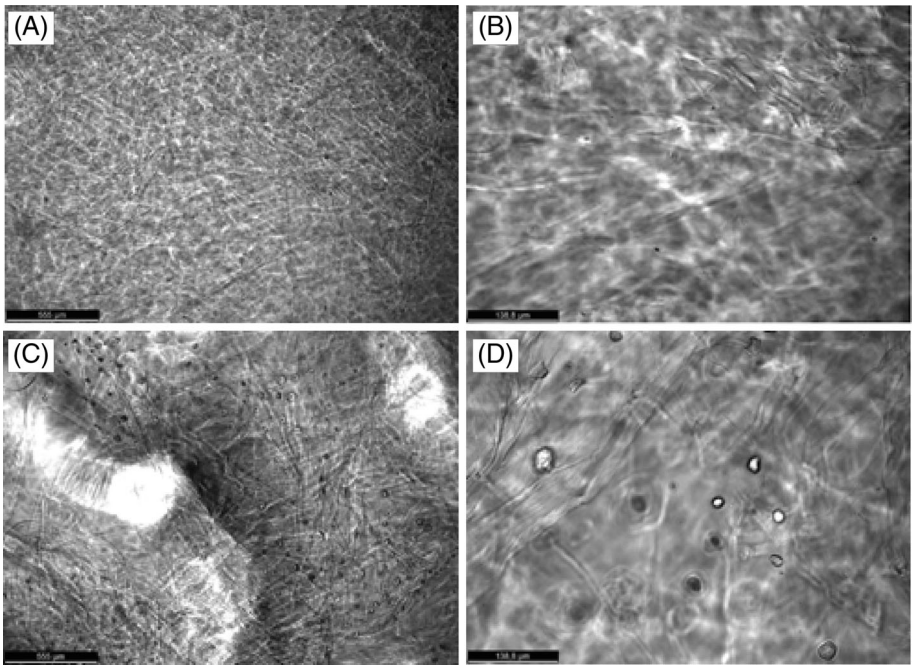

FIGURE 5 Light microscopic images of Gellan 1:2 hydrogels alone (A and B), and with NHDF (C and D) after 2 weeks of culture. In subfigures C and D, the round bodies highlight the presence of fibroblasts (NHDF). The left panel subfigures A and C were magnified 50×, with a scale bar of 555 μm, whereas the right panel subfigures B and D were magnified 200×, with a scale bar of 138.8 μm.

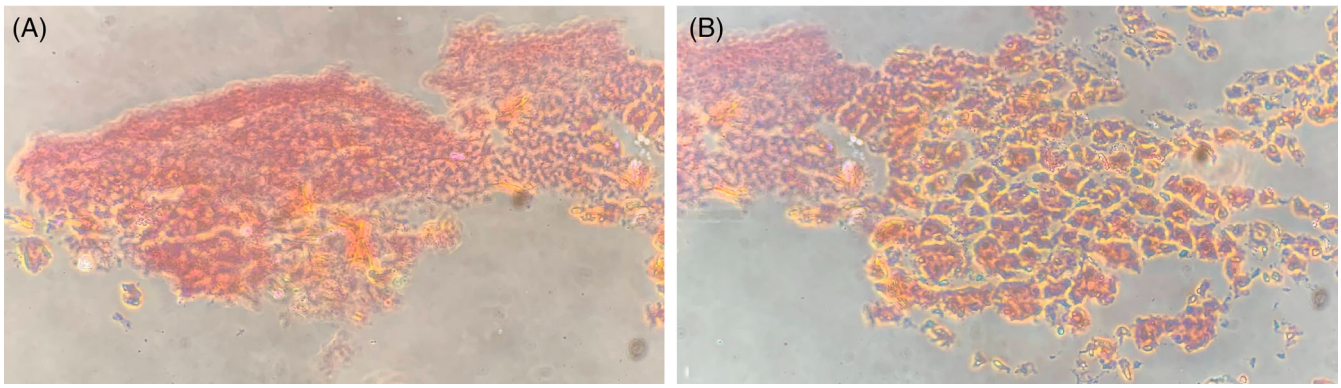

FIGURE 6 Light microscopic images of hematoxylin and eosin (H&E) stained Gellan 1:2 hydrogels with NHDF. The hydrogels were kept in a culture for 2 weeks and then stained with the histological stain. Subfigures A and B show some indication of the formation of an extracellular matrix (ECM; eosin stained in pink), along with fibroblasts' nuclei (hematoxylin stained in purple) in traces.

abbreviated as H&E or simply HE staining, are the common staining dyes in this case. Hematoxylin, a basic or cationic dye, stains the cellular nuclei blue or purple, whereas the cytoplasm and ECM are stained pink or red by the acidic or anionic dye eosin.[40,41] The results of our histological analysis, that is, H&E staining of the samples, are shown in Figure 6A,B. They indicate some signs of ECM formation (visible as pink parts), along with cell nuclei in purple. However, these observations could only be obtained in a couple of slide sections. Hence, the results could not be reproduced. This could be because of the absence of bioactive materials such as ligands, gelatin or collagen in the gellan gum scaffold, which is a microbial polysaccharide. Their presence promotes cell adhesion, proliferation and differentiation.[42,43]

Microstructural studies in combination with a mechanical analysis is critical for a better understanding of human tissues[18,22,44] and therefore, for the development of substitutes for these tissues. Hence, we incorporated and combined these studies in the current work.

3.3 | Permeation attributes

A caffeine diffusion study was carried out to determine the barrier function of these gellan gum hydrogels in two different concentrations, with and without the incorporation of NHDF for 6 h. These were then compared to native human skin, 3D skin models and the κ-carrageenan-based hydrogels analyzed in our study Malhotra et al.[26] Caffeine is proposed as a reference compound in cutaneous absorption studies because of its hydrophilicity.[32] According to OECD guidelines, we represent the penetration data as a percentage in the form of the caffeine amount penetrated over time for a period of 6 h duration. This is shown in Figure 7A, which compares all the specimens in our current study. It can be observed that all the samples show an almost linear dependence. A similar trend has also been reported in other studies performed using different films, such as polymer/polysaccharide-based skin scaffolds, transdermal permeation,

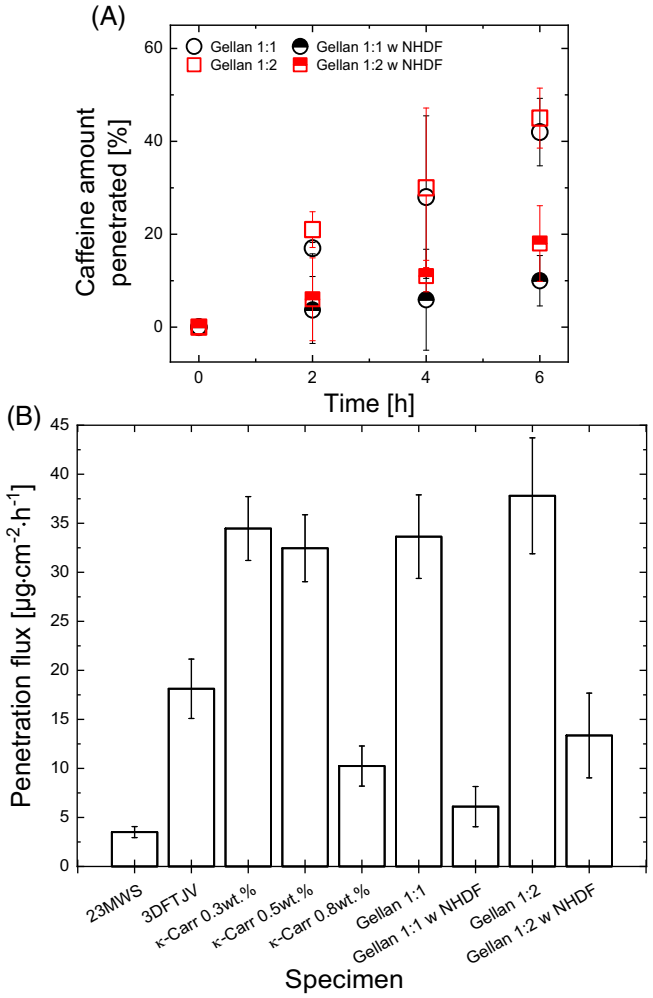

FIGURE 7 Subfigure A shows the permeated amount (in %) of caffeine through both concentrations of gellan gum hydrogels with (semi closed symbols) and without NHDF (open symbols) as a function of time in hours. Subfigure B depicts the penetration flux through gellan gum hydrogels (with and without NHDF) and their comparison to the native benchmark human abdominal skin from a 23-year-old male (23MWS), a commercially available *in vitro* 3D reconstructed juvenile skin model (3DFTJV) and three representative hydrogel variants of κ-carrageenan containing hydrogels, representing the slope of the linear least squares fitting of the data in subfigure A. The error bars represent the standard deviation corresponding to three measurements ($n = 3$). The sample codes and hydrogel compositions are explained in Table 1.

and also simple membrane filters.[32,45] It has previously been shown that a period of 3 h (*ex vivo* human epidermis and 3D epidermis model) to 6 h (polysulfone membrane) is enough to conduct caffeine diffusion tests.[27,46]

As stated in Malhotra et al.,[26] both the 3D skin models and the laboratory fabricated κ-carrageenan-based hydrogels showed higher penetration rates than the native human skin sample. If we compare these results with the gellan gum hydrogels, without fibroblasts, we observe similar penetration parameters over time as shown in Figure 7A. These are comparable with the 0.3 and 0.5 wt % hydrogels containing κ-carrageenan. More than 40% of caffeine permeated through these gels in 6 h, which is almost 10 times the native skin value. Another observation is that the 1:1 ratio gellan hydrogel sample results in a lower penetration amount than the 1:2 ratio specimen. This is the result of a denser polysaccharide network in the 1:1 hydrogel, due to the higher amount of gellan gum polymer in the final solution. A denser polymer network offers smaller pores for the passage of the caffeine solution. Moxon and Smith also discuss the dependency of porosity and permeability on varying crosslinking agents as well as polymer concentration.[5]

However, the gellan gum hydrogels with cultured cells in them show a different scenario altogether. The gellan gum sample that had a 1:1 ratio with incorporated NHDF came close to the native human skin. The 1:2 samples with fibroblasts also show a drastic decrease as compared to their 1:2 hydrogel counterpart, and come closer to the 0.8 wt % κ-carrageenan hydrogels.[26] However, owing to a lower final concentration of gellan gum in 1:2 hydrogels than 1:1 samples, the caffeine penetrated amount through 1:2 gels with NHDF is still higher than that through their 1:1 counterpart. This is because the presence of cells fills the pores formed in the entangled polymer network. This somewhat reduces the passage of the diffusing solution. The increased barrier function of the hydrogels containing dermal fibroblasts can be due to the fact that cells absorb caffeine. Caffeine is a hydrophilic plant alkaloid, and therefore is distributed in the intracellular plasma by binding to plasma proteins. On the other hand, caffeine is also lipophilic and manages to pass through all biological membranes. This can result in the lower penetrated amount observed in the hydrogels containing NHDF.

A clearer picture appears if we take penetration flux into account, which is independent of the penetration area as well as the time allowed for caffeine permeation. Accordingly, the flux was plotted on the y-axis against each specimen on the x-axis, as shown in Figure 7B. 3D skin models showed a penetration flux of 5.2 times the human skin benchmark, which matched the literature value of these models compared to *ex vivo* pig skin.[32] This factor can be called the permeability factor, and can be used to compare various samples with one another, based on their differences from native human skin. Gellan gum-based hydrogels with a ratio 1:1 containing cultured NHDF came close to the native skin and showed a factor of 1.7, whereas the ones with the same ratio but without cells had a factor of 9.6. When the concentration of gellan gum was reduced from 50 v/v% to 33.33 v/v % in the 1:2 sample, the factor increased to 3.8 and 10.8 with and without NHDF respectively. This shows that both samples with cells show a factor value lower than that of the commercially available 3D reconstructed skin models. 0.8 wt % κ-carrageenan-based hydrogels were in between the 1:1 and 1:2 samples with NHDF with a permeability factor of 2.9.

We carried out a statistical analysis of the penetration flux on a population of nine samples (represented in Figure 7B) by a one-way analysis of variance (ANOVA). The significance level was set at .05. It was determined that the group means of all specimens were significantly different as a whole population ($p < .05$). A Tukey test was performed on sample pairs to obtain mean comparisons for all the samples containing dermal cells, including native human skin, 3D skin

TABLE 3 Mean comparisons in pairs of all samples containing dermal cells, and additionally 0.8 wt % κ-carrageenan-based hydrogel scaffold.

Sample pairs for mean comparisons	Significantly different	Significance level
κ-Carr 0.8 wt % – 23MWS	Yes	*
Gellan 1:1 w NHDF – 23MWS	No	
Gellan 1:1 w NHDF – κ-Carr 0.8 wt %	No	
Gellan 1:2 w NHDF – 23MWS	Yes	***
Gellan 1:2 w NHDF – κ-Carr 0.8 wt %	No	
Gellan 1:2 w NHDF – Gellan 1:1 w NHDF	Yes	*
3DFTJV – 23MWS	Yes	*****
3DFTJV – κ-Carr 0.8 wt %	Yes	**
3DFTJV – Gellan 1:1 w NHDF	Yes	***
3DFTJV – Gellan 1:2 w NHDF	No	

Note: Significance level between groups was set for $^{*}p < .05$, $^{**}p < .01$, $^{***}p < .001$, $^{****}p < .0001$, $^{*****}p < .00001$.

models, gellan gum hydrogels with NHDF, and also a 0.8 wt % κ-carrageenan-based hydrogel scaffold from our previous study that achieved the lowest barrier function. This is summarized in Table 3. It was found that only Gellan 1:1 w NHDF sample (highlighted in green) showed no significant difference to native human skin, whereas Gellan 1:2 w NHDF sample (highlighted in blue) matched the value of 3D skin models.

The presence of a permeability factor between skin substitutes and *ex vivo* human skin samples is in agreement with the pertinent literature, where a much higher penetration rate is reported in epidermis-only and full-thickness (FT) artificial skin models than the human skin.[30] There have always been efforts made to decrease this factor. Our study did not achieve the native skin feature, but we were successful in coming closer to it than the values reported in the state of the art. Not only this, our values were better than the full-thickness 3D skin models that are the industry standard. The absence of a complex structure, blood vessels, follicles, glands, blood flow, continuous lipid layer, and metabolism in skin substitutes results in differences from the *in vivo* native skin results.

4 | CONCLUSIONS

We reported on polysaccharide-based, that is, gellan gum-based, hydrogels that are relevant for use as skin substitutes. These hydrogels were incorporated with normal human dermal fibroblasts (NHDF) and cultured for a maximum of 3 weeks. The viscoelastic and penetration properties of the resulting hydrogels were studied. The hydrogel composition and protocol reported here shows a quick, cheap and simple system to achieve crosslinking and incorporation of dermal fibroblasts. The crosslinking of gellan gum was achieved at a physiological temperature of 37°C by adding the cell and tissue culture medium DMEM containing a sufficient amount of the essential cations. The elastic properties of these simplified 3D skin models showed a proximity to the *ex vivo* native human skin samples measured previously and reported in literature.

Microscopic observations of the hydrogels were also documented. A crosslinked, homogeneous network structure of the hydrogels was confirmed by viewing them under a light microscope. NHDF were found dispersed throughout the network. The viability of the fibroblasts was confirmed by a calcein AM fluorescent stain up to a period of 2 weeks of culture. The hydrogels with a higher polymer concentration had a lower cell density due to the lower interstitial space for the incorporation of cells. The histological H&E staining of the hydrogels with cells succeeded in showing traces of the formation of ECM in a small section.

When diffusion properties are considered, the caffeine penetration properties realized in one of the systems containing NHDF showed a smaller permeability factor (1.7 times). This was much closer to its native counterpart, that is, human skin, compared to what we had seen before in commercially available 3D skin models as well as in the multicomponent hydrogel system reported previously by us. As a conclusion, we were successful in establishing a simple system of skin substitutes that displayed a mechanical and penetration compatibility to the native human skin. For further improvement, a functionalisation of the scaffold with a specific amino acid group sequence (RGD) present in the protein collagen can be induced, or gelatin can be added to the scaffold to promote the adhesion and proliferation of cells.[42,47] Additionally, the results could be improved by introducing flow chambers, replacing the static culture.[48] Both oral and dermal fibroblasts showed phenotype changes under a physiologically relevant fluid flow in a quasi *in vivo* bioreactor system that matched *in vivo* behavior.[49]

ACKNOWLEDGMENTS

We are thankful to Ms. Laura Beltran Sangüesa from the Chair of Livestock Biotechnology, TUM for her initial help during the H and E staining of the samples. We would also like to thank Ms. Lana Vidal from the Chair of Brewing and Beverage Technology, TUM for her excellent assistance with the HPLC measurements.

CONFLICT OF INTEREST STATEMENT

The authors declare no conflicts of interest.

DATA AVAILABILITY STATEMENT

The data that supports the findings of this study are available in the supplementary material of this article.

ORCID

Ehsan Fattahi https://orcid.org/0000-0002-9189-493X

REFERENCES

1. Li Z, Lin Z. Recent advances in polysaccharide-based hydrogels for synthesis and applications. *Aggregate*. 2021;2:1-26.
2. Caliari SR, Burdick JA. A practical guide to hydrogels for cell culture. *Nat Methods*. 2016;13(5):405-414.

3. Tibbitt MW, Anseth KS. Hydrogels as extracellular matrix mimics for 3D cell culture. *Biotechnol Bioeng*. 2009;103:655-663.
4. Morris ER, Nishinari K, Rinaudo M. Gelation of gellan – a review. *Food Hydrocoll*. 2012;28:373-411.
5. Moxon SR, Smith AM. Controlling the rheology of gellan gum hydrogels in cell culture conditions. *Int J Biol Macromol*. 2016;84:79-86.
6. Oliveira JT, Martins L, Picciochi R, et al. Gellan gum: a new biomaterial for cartilage tissue engineering applications. *J Biomed Mater Res A*. 2010;93(3):852-863.
7. Alheib O, da Silva LP, Youn YH, Kwon IK, Reis RL, Correlo VM. 3D bioprinting of gellan gum-based hydrogels tethered with laminin-derived peptides for improved cellular behavior. *J Biomed Mater Res A*. 2022;110(10):1655-1668.
8. Joglekar MM, Ghosh D, Anandan D, et al. Crosslinking of gum-based composite scaffolds for enhanced strength and stability: a comparative study between sodium trimetaphosphate and glutaraldehyde. *J Biomed Mater Res*. 2020;108(8):3147-3154.
9. Lee H, Fisher S, Kallos MS, Hunter C. Optimizing gelling parameters of gellan gum for fibrocartilage tissue engineering. *J Biomed Mater Res*. 2011;98(2):238-245.
10. Li W, Jian X, Zou Y, et al. The fabrication of a gellan gum-based hydrogel loaded with magnesium ions for the synergistic promotion of skin wound healing. *Front Bioeng Biotechnol*. 2021;9:709679.
11. Manda MG, da Silva LP, Cerqueira MT, et al. Gellan gum-hydroxyapatite composite spongy-like hydrogels for bone tissue engineering. *J Biomed Mater Res A*. 2018;106(2):479-490.
12. Silva-Correia J, Oliveira JM, Caridade SG, et al. Gellan gum-based hydrogels for intervertebral disc tissue-engineering applications. *J Tissue Eng Regen Med*. 2011;5:97-107.
13. Xu Z, Zhang L, Bentil SA, Bratlie KM. Gellan gum-gelatin viscoelastic hydrogels as scaffolds to promote fibroblast differentiation. *Mater Sci Eng C*. 2021;129:112370.
14. Zhang L, Zheng T, Wu L, et al. Fabrication and characterization of 3D-printed gellan gum/starch composite scaffold for Schwann cells growth. *Nanotechnol Rev*. 2021;10:50-61.
15. Loebel C, Mauck RL, Burdick JA. Local nascent protein deposition and remodelling guide mesenchymal stromal cell mechanosensing and fate in three dimensional hydrogels. *Nat Mater*. 2019;18(8):883-891.
16. Wells RG. The role of matrix stiffness in regulating cell behavior. *Hepatology*. 2008;47:1394-1400.
17. Murugan R, Ramakrishna S. Design strategies of tissue engineering scaffolds with controlled fiber orientation. *Tissue Eng*. 2007;13:1845-1866.
18. Geerligs M, Oomens C, Ackermans P, Baaijens F, Peters G. Linear shear response of the upperskin layer. *Biorheology*. 2011;48:229-245.
19. Holt B, Tripathi A, Morgan J. Viscoelastic response of human skin to low magnitude physiologically relevant shear. *J Biomech*. 2008;41:2689-2695.
20. Lamers E, Kempen VT, Baaijens FP, Peters GW, Oomens CW. Large amplitude oscillatory shear properties of human skin. *J Mech Behav Biomed Mater*. 2013;28:462-470.
21. Lynch B, Pageon H, Le Blay H, et al. A mechanistic view on the aging human skin through ex vivo layer-by-layer analysis of mechanics and microstructure of facial and mammary dermis. *Sci Rep*. 2022;12:849.
22. Malhotra D, Pan S, Rüther L, et al. Linear viscoelastic and microstructural properties of native male human skin and in vitro 3D reconstructed skin models. *J Mech Behav Biomed Mater*. 2019;90:644-654.
23. Wang L, Wang C, Wu S, Fan Y, Li X. Influence of the mechanical properties of biomaterials on degradability, cell behaviors and signaling pathways: current progress and challenges. *Biomater Sci*. 2020;8:2714-2733.
24. Almeida N, Mueller A, Hirschi S, Rakesh L. Rheological studies of polysaccharides for skin scaffolds. *J Biomed Mater Res A*. 2014;102:1510-1517.
25. Dąbrowska AK. *From the Characterization of Human Skin to the Development of a Skin Model*. ETH Zürich; 2017.
26. Malhotra D, Pan S, Rüther L, Schlippe G, Voss W, Germann N. Polysaccharide-based skin scaffolds with enhanced mechanical compatibility with native human skin. *J Mech Behav Biomed Mater*. 2021;122:104607.
27. Casiraghi A, Ranzini F, Musazzi UM, Franze S, Meloni M, Minghetti P. In vitro method to evaluate the barrier properties of medical devices for cutaneous use. *Regul Toxicol Pharmacol*. 2017;90:42-50.
28. Luo L, Lane ME. Topical and transdermal delivery of caffein. *Int J Pharm*. 2015;490:155-164.
29. Abd E, Yousef SA, Pastore MN, et al. Skin models for the testing of transdermal drugs. *Clin Pharmacol Adv Appl*. 2016;8:163-176.
30. Neupane R, Boddu SH, Renukuntla J, Babu RJ, Tiwari A. Alternatives to biological skin in permeation studies: current trends and possibilities. *Pharmaceutics*. 2020;12(2):1-25.
31. Zacchi V, Soranzo C, Cortivo R, Radice M, Brun P, Abatangelo G. In vitro engineering of human skin-like tissue. *J Biomed Mater Res*. 1998;40(2):187-194.
32. Ackermann K, Lombardi Borgia S, Korting HC, Mewes KR, Schäfer-Korting M. The Phenion® full-thickness skin model for percutaneous absorption testing. *Skin Pharmacol Physiol*. 2010;23:105-112.
33. Pan S, Malhotra D, Germann N. Nonlinear viscoelastic properties of native male human skin and in vitro 3D reconstructed skin models under LAOS stress. *J Mech Behav Biomed Mater*. 2019;96:310-323.
34. Feng Y, Dai S-C, Lim K, Ramaswamy Y, Jabbarzadeh A. Tribological and rheological properties of poly(vinyl alcohol)-gellan gum composite hydrogels. *Polymers*. 2022;14:3830.
35. Rivero RE, Capella V, Liaudat AC, et al. Mechanical and physicochemical behavior of a 3D hydrogel scaffold during cell growth and proliferation. *RSC Adv*. 2020;10:5827-5837.
36. Schultz KM, Kyburz KA, Anseth KS. Measuring dynamic cell–material interactions and remodeling during 3D human mesenchymal stem cell migration in hydrogels. *Proc Natl Acad Sci USA*. 2015;112:3757-3764.
37. Donati I, Asaro F, Paoletti S. Experimental evidence of counterion affinity in alginates: the case of nongelling ion Mg2+. *J Phys Chem B*. 2009;113(39):12877-12886.
38. Jahromi SH, Grover LM, Paxton JZ, Smith AM. Degradation of polysaccharide hydrogels seeded with bone marrow stromal cells. *J Mech Behav Biomed Mater*. 2011;4:1157-1166.
39. Munoz-Espin D, Serrano M. Cellular senescence: from physiology to pathology. *Nat Rev Mol Cell Biol*. 2014;15(7):482-496.
40. Chan JK. The wonderful colors of the hematoxylin-eosin stain in diagnostic surgical pathology. *Int J Surg Pathol*. 2014;22(1):12-32.
41. Wittekind D. Traditional staining for routine diagnostic pathology including the role of tannic acid. 1. Value and limitations of the hematoxylin-eosin stain. *Biotech Histochem*. 2003;78(5):261-270.
42. Chen H, Zhang Y, Ding P, et al. Bone marrow-derived mesenchymal stem cells encapsulated in functionalized gellan gum/collagen hydrogel for effective vascularization. *ACS Appl Bio Mater*. 2018;1:1408-1415.
43. Ng JY, Obuobi S, Chua ML, et al. Biomimicry of microbial polysaccharide hydrogels for tissue engineering and regenerative medicine – a review. *Carbohydr Polym*. 2020;241:116345.
44. Zak M, Kuropka P, Kobielarz M, Dudek A, Kaleta-Kuratewicz K, Szotek S. Determination of the mechanical properties of the skin of pig foetuses with respect to its structure. *Acta Bioeng Biomech*. 2011;13(2):37-43.
45. Kim C, Shim J, Han S, Chang I. The skin-permeation-enhancing effect of phosphatidylcholine: caffeine as a model active ingredient. *J Cosmet Sci*. 2002;53:363-374.
46. Mustapha RB, Lafforgue C, Fenina N, Marty JP. Influence of drug concentration on the diffusion parameters of caffeine. *Indian J Pharmacol*. 2011;43:157-162.
47. Miranda-Nieves D, Chaikof EL. Collagen and elastin biomaterials for the fabrication of engineered living tissues. *ACS Biomater Sci Eng*. 2017;3(5):694-711.

48. Mammoto T, Ingber DE. Mechanical control of tissue and organ development. *Development*. 2010;137:1407-1420.
49. Nithianantha S, Crawford A, Cooper Knock J, Lambert DW, Whawell SA. Physiological fluid flow moderates fibroblast responses to TGFβ-1. *J Cell Biochem*. 2017;118:878-890.

SUPPORTING INFORMATION

Additional supporting information can be found online in the Supporting Information section at the end of this article.

How to cite this article: Malhotra D, Fattahi E, Germann N, Flisikowska T, Schnieke A, Becker T. Skin substitutes based on gellan gum with mechanical and penetration compatibility to native human skin. *J Biomed Mater Res*. 2023;111(10): 1588-1599. doi:10.1002/jbm.a.37557